DFT Studies of Solvation Effects on the Nanosize Bare, Thiolated, and Redox Active Ligated Au_{55} Cluster†

Ganga Periyasamy,† Engin Durgun,‡ Jean-Yves Raty,‡ and F. Remacle*,†

Department of Chemistry, Bat. B6c, University of Liège, B4000 Liege, Belgium, and Department of Physics, Bat. B5, University of Liège, B4000 Liege, Belgium

Received: December 18, 2009; Revised Manuscript Received: March 11, 2010

The structural and electronic properties of the bare Au_{55} cluster, and of the model thiol passivated $Au_{55}(SCH_3)_{42}$, the redox active ligated $Au_{55}S(CH_2)_2CO_2(CH_2)_{10}bpy\cdot 2Cl$ and $Au_{55}(SCH_3)_{41}(S(CH_2)_2CO_2(CH_2)_{10}bpy)\cdot 2Cl$ (bpy = *N*-methyl-4,4′-bipyridinium) complexes are studied at the DFT level in the gas phase and with an explicit water layer. For all complexes, neutral, positive, and negative charge states are investigated. The thiol ligation distorts the outer layer of the approximate icosahedral geometry of the bare cluster and induces a charge transfer from the gold core to the ligand shell. The anchoring of a single redox active ligand on the bare Au_{55} leads to the formation of a cavity around the S−Au bond. We show that this cavity formation is prevented by the thiol ligands in $Au_{55}(SCH_3)_{41}(S(CH_2)_2CO_2(CH_2)_{10}bpy)\cdot 2Cl$. The vertical addition of one electron to the $[Au_{55}\ S(CH_2)_2CO_2(CH_2)_{10}bpy\cdot 2Cl]^0$ cluster is followed by a charge transfer from the Au_{55} core to the bpy^{2+} ligand, which is accompanied by a mechanical motion of the redox active bpy arm driven by electrostatic interactions. The presence of a solvent shell does not alter the structure but significantly decreases the computed charging energies of the clusters, making them comparable with experimental values. The computed redox potential differences are in good agreement with the experimental values.

Introduction

Gold clusters exhibit a rich array of interesting electronic, optical, chemical, and catalytic properties, typically with a sharp size threshold, that has sparked a huge interest in several areas. For example, gold particles are catalytically active when their diameter falls below 2 nm and completely inactive above. Among small size gold nanoparticles (NP), Au_{55} clusters possess an ideal size (1.4 nm) for catalytic activity, a full shell geometry, and oxidation-resistant properties.[1−5]

Gold Au_{55} nanoclusters are not stable in the bare form and need to be stabilized by ligand layers such as in $Au_{55}(PPh_3)_{12}Cl_6$,[6] $Au_{55}(BSH)_{12}^{2+}$,[7] $Au_{55}(SC_n)_{32}$ clusters (chain length n = 12, 18),[8] $Au_{55}(T_8\text{-O-SS-SH})_{12}C_{l6}$,[9] and $Au_{55}(Ph_2PC_6H_4SO_3Na)_{12}Cl_6$,[6] etc. They can self-assemble into one-, two-, and three-dimensional arrays,[4,10−12] and because of their large charging energies (0.3−0.5 eV) they can operate as single electron devices at room temperature,[1] which makes them suitable for applications in nanoelectronics.[4] In addition, one can also anchor redox active molecules in the ligand shell to increase their functionalities.[13−15] When used in catalysis or electrocatalysis, as chemical sensors or electronic components, these hybrid nanoclusters are often surrounded by solvent molecules.[16,17] The water layer as well as the chemical nature of the ligands were shown to strongly affect their electronic properties.[3,15,18,19]

We report on a systematic computational study of these effects at the DFT level of theory. We first investigate the structural and electronic properties of the bare Au_{55} cluster in neutral, positive, and negative charge states and the effect of an explicit water layer of 54 solvent molecules. We then explore the effect of a densely packed outer layer of passivating SCH_3 ligands, with and without a water layer, on the three charge states. We finally replace one of the SCH_3 by the redox active $S(CH_2)_2CO_2(CH_2)_{10}bpy^{2+}.2Cl$ and compare its properties with those of a Au_{55} cluster bonded to a single $S(CH_2)_2CO_2(CH_2)_{10}bpy^{2+}\cdot 2Cl$, to quantify the stabilization effect of the thiol layer on the geometry and to estimate how this layer affects the redox properties of the complex. The properties of the two complexes, $Au_{55}(SCH_3)_{41}(S(CH_2)_2CO_2(CH_2)_{10}bpy^{2+})\cdot 2Cl$ and $Au_{55}S(CH_2)_2CO_2(CH_2)_{10}bpy^{2+}\cdot 2Cl$ were also studied in the presence of a partial water layer of 21 molecules. Our choice of $Au_{55}(SCH_3)_{42}$ that has not been observed experimentally is motivated by the fact that the thiol layer is densely packed and is a good model of the densely packed short self-assembled monolayer that was used in the CV measurements of the redox properties of the bpy ligand by Willner et al.[13]

We also report on computations $Au_{55}(SCH_3)_{32}$, a model for the $Au_{55}(SC_{18})_{32}$ cluster experimentally identified[8] where the dilution of the ligand shell leads to the formation of Au−S−Au bridges. The formation of such bridges has been reported at the experimental and computational levels for other cluster sizes, for example, $Au_{102}(SR)_{44}$[20,21] and $Au_{25}(SR)_{18}^{-}$[22−24] for which crystallographic data are available, and on the EI-MS resolved $Au_{38}(RS)_{24}$[25−29] and $Au_{144}(RS)_{60}$.[30,31]

On the theoretical side, there is an intense research effort to characterize the properties of gold clusters of various sizes, ligand shells, and charge states using both quantum chemistry and solid-state DFT methods[12,21,23,28,32−39] (for recent reviews, see refs 29, 40, and 41 and references therein). For large cluster sizes, larger than a few dozen atoms, parameter-free electronic-structure methods cannot be applied to perform an unbiased structure optimization because of the large computational resources needed. Instead one has to resort to approximate methods. It turned out that in the case of gold clusters the resulting structures depend on the chosen approximation in a

† Part of the special issue "Protected Metallic Clusters, Quantum Wells and Metallic Nanocrystal Molecules".

* To whom correspondence should be addressed, fremacle@ulg.ac.be.
† Department of Chemistry, Bat. B6c.
‡ Department of Physics, Bat. B5.

10.1021/jp9119827
Published on Web 03/30/2010

very sensitive manner. For this reason, the stability of the structures reported here has been checked using both DFT quantum chemistry and solid state approaches.

This paper is organized as follows. The computational method is described in section II. The structural properties of the bare and of the ligated and solvated clusters in three oxidation states are analyzed in section III. The charge distributions of these clusters are discussed in the section IV. Finally, section V is devoted to their electrical properties and conclusions are given in section VI.

II. Computational Details

Both quantum chemistry and solid-state implementations of density functional theory were used to assess the stability of the geometries of the large hybrid clusters investigated. In both approaches, we use relativistic energy corrected pseudopotentials (RECP) since it has been shown early on that the relativistic effects of gold atoms play an important role in the properties of gold clusters.[32,42,43]

The use of atomic-centered basis functions together with pseudopotentials for the gold atoms and hybrid functionals is well established for this kind of system. However for larger systems this approach becomes increasingly expensive because of the computation of the multicenter electron integrals. It is therefore more efficient to resort to a plane wave expansion combined with pseudopotentials, as implemented in solid-state DFT methods. It is in general easier to relax the geometry of a large cluster, up to thousands of atoms, using the plane wave approach. This is particularly important for the explicit solvation effects studied here which require at least one layer of water molecules around the clusters. On the other hand, the atomic centered basis set approach is better suited for the prediction of the local properties of the system, such as local atomic charges. These are also expected to be sensitive to exchange, which we therefore included in our quantum chemistry calculations using hybrid functionals.

The systems that we study are still small enough to be tackled by both approaches. Our strategy in order to assess the stability of the computed geometries for the solvated large clusters is to first get a converged geometry by the solid-state approach, which is then reoptimized by the methods of quantum chemistry. Both DFT implementations, the VASP plane wave approach using the GGA-PW91 functional and the PAW pseudopotentials, and the Gaussian03 B3LYP/LANL2MB/6-31+G(d) approach lead to consistent results for the structural and electronic properties for the ligated and solvated clusters in different charge states investigated here (see Table S1 of Supporting Information for more details). In particular, both DFT methods converged to the same stable distorted icosahedral geometries and lead to similar energy differences when compared with the higher energy distorted cubahedral isomers.

The quantum chemistry geometry optimizations were carried out using Density Functional Theory as implemented in the Gaussian 03 suite of programs[44] with the hybrid B3LYP functional, the LANL2MB RECP pseudopotential and basis set for gold, and 6-31+G(d) Gaussian basis set for all other atoms. The stationary structures of the three charged states (positive, neutral, and negative) of the bare Au_{55} (Figure 1a) and of the redox inactive thiol ligated $Au_{55}(SCH_3)_{42}$ (Figure 2a) and $Au_{55}(SCH_3)_{32}$ (Figure S2 in Supporting Information) clusters were characterized as minima on the basis of the calculation of their harmonic vibrational frequencies with the options opt = tight (10^{-6} hartree/bohr for the forces on atoms) and SCF = tight (10^{-8} hartree convergence threshold). The electronic structures

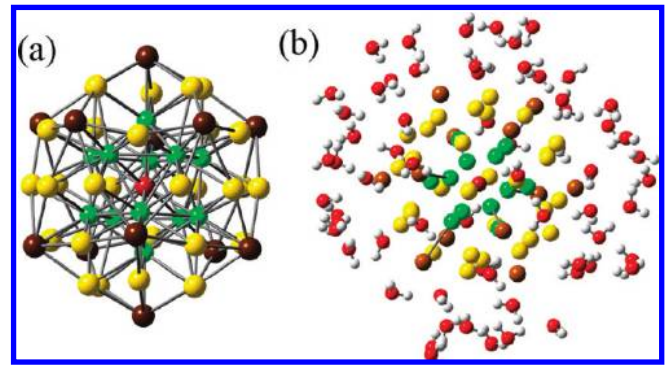

Figure 1. The relaxed geometries of the bare Au_{55} cluster (a) and of the solvated $Au_{55}\cdot 54H_2O$ one (b). Four types of gold atoms are shown in the red, green, yellow, and brown, and the water molecules are shown in the red color.

and equilibrium geometries of the larger solvated clusters, $Au_{55}\cdot 54H_2O$ (Figure 1b), $Au_{55}(SCH_3)_{42}\cdot 54H_2O$ (Figure 2b), $Au_{55}S(CH_2)_2CO_2(CH_2)_{10}bpy\cdot 2Cl$, $Au_{55}S(CH_2)_2CO_2(CH_2)_{10}bpy\cdot 2Cl\cdot 21H_2O$, $Au_{55}(SCH_3)_{41}(S(CH_2)_2CO_2(CH_2)_{10}bpy)\cdot 2Cl$ (Figure 3) were converged with the loose convergence criteria: 10^{-5} hartree for SCF convergence and 10^{-5} hartree/bohr for the root mean square force. For the Au_{55} bare and $Au_{55}(SCH_3)_{42}$ cluster the water molecule layer is added by using Amber tools,[45] while for the $Au_{55}S(CH_2)_2CO_2(CH_2)_{10}bpy\cdot 2Cl$ cluster the water molecules are positioned around the ligand in order to understand specific solvation effects on the bpy redox active unit.

Before initializing the computation in the plane wave approach, we first determined the energy cutoff for the plane wave basis expansion that is required to achieve convergence of the energy and the molecular structure, especially for the charged systems. So we have repeated few computations on the Au_{55} bare, $Au_{55}(SCH_3)_{42}\cdot 54H_2O$ (Figure 2b), $Au_{55}S(CH_2)_2CO_2(CH_2)_{10}bpy\cdot 2Cl$, and $Au_{55}S(CH_2)_2CO_2(CH_2)_{10}bpy\cdot 2Cl\cdot 21H_2O$ (Figure 3a,b) clusters using first-principles plane wave calculations within density functional theory (DFT) as implemented in the VASP package[46,47] with 11 electron relativistic energy corrected PAW[48] potentials in order to find out the convergence criteria. The energy cutoff was assigned to be 550 eV. The exchange correlation potential is approximated by the Generalized Gradient Approximation (GGA-PW91). The GGA approximation for the exchange correlation does not include an explicit Hartree−Fock exchange. It is a density functional that is designed to fit the density dependence of the electronic properties of the electron gas.

We have used a $40 \times 40 \times 40$ Å^3 cell in order to include a sufficiently large vacuum space around the cluster. The self-consistent potential and total energy are calculated at the Gamma point of the Brillouin zone. Ultimately, a plane wave basis set with a maximal kinetic energy of 550 eV has been used. All atomic positions were optimized by performing simultaneous minimizations of the total energy and of the atomic forces using the conjugate gradient method. The convergence on the total system energy in the SCF cycles is chosen as 10^{-5} eV (2.721×10^{-4} hartree) and the maximum force allowed on each atom is 0.05 eV/Å ($=3.6 \times 10^{-3}$ hartree/bohr). In the VASP-DFT calculations on charged systems, a uniform background compensation charge is included and the corrections take into account both point charge, dipole, and quadrupole corrections.

The use of DFT methods in conjunction with relativistic pseudopotential to determine the structure of gold clusters is well established and was shown to give reasonable agreement with experimental values. Various functionals were used in the

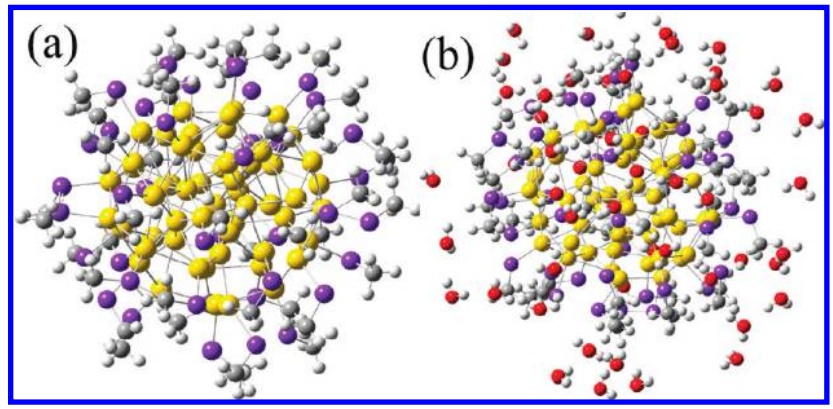

Figure 2. The relaxed geometries of the thiol ligand protected $Au_{55}(SCH_3)_{42}$ (a) and solvated $Au_{55}(SCH_3)_{42}\cdot 54H_2O$ (b) clusters. The atom color coding is the following: yellow, gold; gray, carbon; violet, sulfur; white, hydrogen.

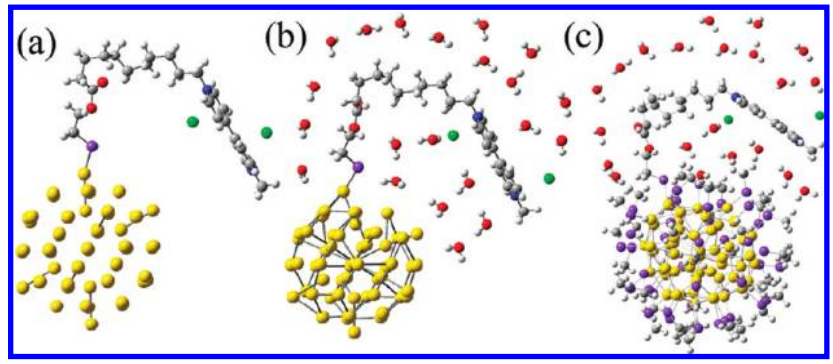

Figure 3. The relaxed geometries of various models with redox active ligand investigated in this paper: (a) $Au_{55}S(CH_2)_2CO_2(CH_2)_{10}$bpy, (b) $Au_{55}S(CH_2)_2CO_2(CH_2)_{10}bpy\cdot$2Cl$\cdot$21$H_2O$, and (c) [$Au_{55}$-$(SCH_3)_{41}$(S-*link*-bpy)$\cdot$2Cl$\cdot$21$H_2O$] where bpy = *N*-methyl-*N*-carboxyethyl-4,4′-bipyridinium. The atom color coding is the following: yellow, gold; violet, sulfur; blue, nitrogen; gray, carbon; green, chlorine; red, oxygen; white, hydrogen.

literature. In the case of hybrid complexes passivated with organic ligands, it was shown that hybrid functionals like B3LYP that include a part of Hartree−Fock exchange usually perform better. The results reported hereafter show that both LANL2MB/B3LYP and PAW/GGA where there is no HF exchange in GGA lead to the same stable structures and electronic properties (see also Table S1 of Supporting Information). This level of theory therefore appears to be a reasonable compromise to tackle the computation of the electronic structure of large solvated metal−organic hybrid complexes.

III. Structural Analysis

The structural analysis of the stable geometries of the bare clusters determined by the solid-state approach confirms the results recently obtained at the LANL2MB/B3LYP level:[49] Au_{55} exhibits a full shell geometrical structure with a complete outer layer and the distorted icosahedral geometry is more stable than the distorted cubahedral (see Figure 4) in the positive, neutral, and negative charge states by 33.24, 30.02, and 29.21 kcal mol^{-1}, respectively. In the distorted icosahedral geometry the central Au atom is surrounded by two layers: a first layer of 12 Au atoms at ∼0.29 nm and a second shell of 42 atoms made of 30 face edge atoms at ∼0.58 nm and of 12 face centered ones at ∼0.51 nm (Figure 4a). Face edge atoms and face center atoms differ by their coordination numbers, which are respectively equal to 6 and 8. Similarly, the distorted cubahedral geometry has a layer-like structure. It is made of five layers: the central layer (labeled 1 in Figure 4b) contains 19 atoms, the next two layers (labeled 2 and 2′ in Figure 4b) are symmetrically arranged about the middle layer and contain 12 atoms each. The two external layers (labeled 3 and 3′ in Figure 4b) contain 6 atoms each.

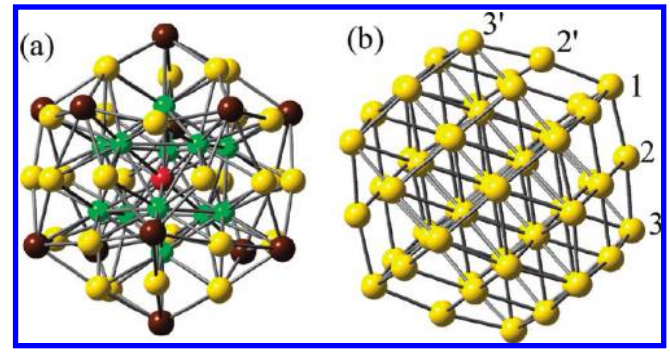

Figure 4. The distorted icosahedral (a) and cubahedral (b) geometries for bare $[Au_{55}]^0$ clusters. For clarity purpose the four different types of gold atoms in icosahedral geometry are shown in the different colors: (i) center gold atom in red, (ii) inner layer gold atoms in green, (iii) outer layer face center atoms in yellow, and (iii) outer layer face edge atoms in brown. The layers of the cubahedral geometry are numbered as referred to in the text. Figure S1 of the Supporting Information shows the six different kinds of atoms characteristic of the cubahedral geometry.

Both isomers exhibit a hexagonal outer layer shape (Figure 4) and a diameter value of 1.15 nm that are agreement with X-ray photoelecton spectroscopy,[43,50,51] scanning tunneling microscopy,[52−54] transmission electron microscopy,[55,56] EXAFS,[57,58] ENDOR,[59] and impedance spectroscopic[2,7] experimental data.[55,60] However, as discussed in section III below, only the more stable icosahedral structure that has four types of different gold atoms (shown in Figure 4 in different colors) is in agreement with the results of Mossbauer spectroscopy.[61] The cubahedral geometry contains six types of atoms, characterized by specific partial charges (see Supporting Information and Figure S1).

Relativistic effects of 5d−6s orbitals of the gold atoms lead to a distortion of the computed geometries of the icosahedral and cubahedral isomers compared to the perfect geometrical shape.[32,42,43,62] Because of a better hybridization of the outer shell face center 6s and face edge 6s orbitals, the negatively charged Au_{55}^- cluster has a less distorted geometry than the neutral and positively charged clusters.[49]

Experimentally, the bare Au_{55} clusters are usually stabilized and crystallized in the presence of ligand and solvent layers, which affect their structural and electronic properties. For ligated clusters, the starting geometry of the Au_{55} core was chosen as the stable icosahedral one. This is supported by our previous computations on the $Au_{55}(PH_3)_{12}Cl_6$ complex where the optimization of cubahedral geometry in the presence of ligands systematically reverts to the distorted icosahedral geometry for all charged states.[49]

We first study the stability of the Au_{55} icosahedral cluster in the presence of a water layer. The effect of solvation can be computed using an implicit dielectric medium or explicit water solvation.[63] Our recent studies on ligated $[Au_{55}(PH_3)_{12}Cl_6]\cdot 54H_2O$ proved the importance of explicit solvation, where the H-bonding between the solvent layer and the chlorine atoms switches the coordination mode between the Au and the Cl atoms.[49] Previous results also showed that a nonconventional H-bond can form between small Au clusters and ligand containing N−H and O−H groups.[64−66] These results lead us to investigate the effect of an explicit single layer of 54 water molecules on the nanosized Au_{55} cluster. While a single layer of water molecules may not be enough to completely solvate the gold cluster, it allows us to closely investigate the bonding patterns between the outer shell gold atoms and the water molecules. On average in $Au_{55}\cdot 54H_2O$, three nonconventional weak Au···H−OH H-bonds per surface gold atom are present for all charge states, positive, neutral, and negative, but no covalent Au−O bonds are formed unlike in smaller hybrid complexes.[64,65] The computed diameter of the Au_{55} core increases from 1.15 in the bare form to 1.22 nm in $Au_{55}\cdot 54H_2O$ for all three $[Au_{55}\cdot 54H_2O]^+$, $[Au_{55}\cdot 54H_2O]^0$, and $[Au_{55}\cdot 54H_2O]^-$ complexes, reflecting a non-negligible charge transfer from the gold core to the ligand shell. The strengths of the nonconventional H-bonds depend on the negative charge of the outer shell gold atoms. In the negatively charged cluster, the average Au···H−O bond length slightly decreases (typically by ∼0.2 Å) because of the larger partial negative charge on the outer layer. Note that the water layer does not penetrate into the Au_{55} cluster, so that the full shell geometrical structure is preserved under explicit solvation by a water layer. We did not observe any Au−O bond formation during the geometry relaxation.

We then turn to the influence of thiol ligation (by SCH_3) on the distorted icosahedral structure of the Au_{55} cluster. The $Au_{55}(SCH_3)_{42}$ cluster where each outer shell (face centered and face edged) gold atoms are covalently bonded to one of the thiol ligand is studied using an atomic center basis set approach. This cluster can be a model for the larger thiol passivated $Au_{55}(SCH_2COOPh)_{42}$ nanocluster. Thiol ligation highly distorts the geometry of the outer layer of Au_{55}. In the stable geometry, the sulfur atoms are covalently bound, making Au−S bonds with the outer layer gold atoms of 2.12−2.40 Å, depending on the charge state. This is unlike the RS−Au−SR and RS−Au−RS−Au−SR coordination motifs that have been identified in the crystallographically resolved thiolate protected $Au_{102}(SR)_{44}$[20,21] and in crystallographically and EI-MS resolved $Au_{25}(SR)_{18}$[22−24] as well as in the EI-MS resolved $Au_{38}(SR)_{24}$[25−29] and $Au_{144}(SR)_{60}$[30,31] clusters.

The different ligation in $Au_{55}(SCH_3)_{42}$ reported here is due to the full shell geometrical structure of the Au_{55} and the densely packed thiol layer. We also investigated the structure of the more diluted ligand shell in $Au_{55}(SCH_3)_{32}$ cluster, which has been studied experimentally[8] but for which no EI-MS characterization or crystallographic structure is available. The geometry optimization of the positive, neutral, and negatively charged states was initialized with single Au−S coordination. The structural relaxation leads to the formation of asymmetric RS−Au−SR coordination with 2.42−2.54 and 2.95−3.12 Å distances depending upon the charge state (see Figure S2 in Supporting Information). In addition, the integrity and hexagonal shapes of the Au_{55} core are preserved with four types of gold atoms as for the denser ligand shell. However several conformers are possible for the anchoring of the redox active ligand. Our motivation here is to understand the effect of the charge state on the redox active ligand, in relation with the experiment of Willner at al[13] on a densely packed self-assembled monolayer, for which the densely packed $Au_{55}(SCH_3)_{42}$ turns out to be a good model.

The densely packed thiol groups prevent the formation of a nonconventional H-bond between the Au_{55} outer layer and the CH_3 groups in all three charge states. On the other hand, strong S···H−S H-bonding occurs within the SCH_3 layer. Similarly to the Au_{55} bare clusters, the geometry of the negatively charged ligated $[Au_{55}(SCH_3)_{42}]^-$ cluster is less distorted than the neutral and positively charged ones. The ligand passivation increases the diameter of the Au_{55} core by 0.2 nm, which is slightly more than that for the solvated $Au_{55}\cdot 54H_2O$ cluster.

Most of the experimental studies of ligand-protected nanoclusters are carried out in solution, where the solvent can influence the geometry and stabilization of the passivated Au_{55} cluster. The water solvation was chosen in order to mimic the redox reaction in the CV experiments. Solvent effects on the thiolated $Au_{55}(SCH_3)_{42}$ are taken into account by adding one layer of explicit 54 water molecules around the $Au_{55}(SCH_3)_{42}$ cluster. Both atomic center basis set and the plane wave geometry optimizations were carried out in that case. The computations show that the dense passivation provided by the thiol layer blocks any direct interaction between water molecules and the outer layer of gold atoms. However solvation slightly weakens the Au−S bonds (their length increases by 0.01 Å, as observed in the local orbital basis/hybrid functional approach). The reason is that the thiol groups and the water molecules engage in a tight H-bond interaction network.

Anchoring of Redox Active Ligand. Recent studies report on functionalized ligated nanoclusters, where redox or optically active ligands are anchored on the nanocluster.[67−76] Functionalized nanoclusters are expected to play an important role in molecular electronics and can be useful to understand electrochemical reactions occurring in the self-assembled monolayers. We chose to study the anchoring of the redox active ligand *N*-methyl-4,4′-bipyridinium (bpy^{2+}) on Au_{55} clusters via thiol linkage. We are particularly interested in the reported[13] "mechanical arm" motion toward the electrode surface induced by electrochemical pulse. In ref 13 the mechanical arm motion is triggered by changing the charge at the gold surface, and it is due to charge−charge attraction and repulsion between the charged gold surface and the redox active bpy ligands. This can be modeled by changing the charge at the Au_{55} nanocluster.

The structure and electronic properties of the isolated redox active ligands were first studied using the atomic center basis

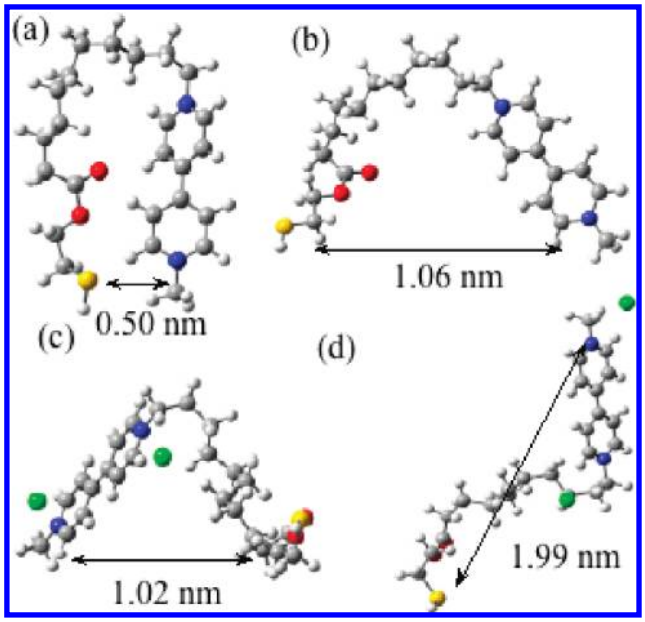

Figure 5. Stationary structures of dication (bpy^{2+}: a, c) and monocation radical ($bpy^{\bullet+}$: b, d) form of the thiol bpy ligand in the absence and presence of counter-chlorine ions computed in the gas phase. In the monocation structure (d), the unpaired electron is localized on the bpy unit (see Figure S3 in Supporting Information) and the distance between bpy and the thiol group increases because of electrostatic repulsion. As a result one of the Cl counterions is forming an H-bond with activated hydrogen of a neighboring CH_2 unit. The atom color coding is the following: blue, nitrogen; gray, carbon; yellow, sulfur; green, chlorine; red, oxygen; white, hydrogen.

function approach. The bipyridinium (bpy) thiol ligand molecule is redox active with a single redox dication/monoradical cation couple: $bpy^{2+}/bpy^{\bullet+}$. The structural change during this redox process was studied for two charge states (+2 and +1) of an isolated $HS(CH_2)_2CO_2(CH_2)_{10}$bpy molecule in the gas phase, in the presence and absence of counterions (chlorine) (see Figure 5). In the dication, bpy^{2+}, the hole made by removing the unpaired electron is localized on the bpy head; see Figure S3 in Supporting Information. The dication (bpy^{2+}), parts a and c of Figure 5, has therefore a more folded form than the monoradical cation. The changes in folding are reflected by the distance between the tail thiol group and bpy unit (see Figure 5). The presence of counter-chlorine ions increases the distance between the thiol group and the bpy unit for the dicationic form and leads to a completely unfolded structure for the monocation (see Figure 5). This is due to the screening effect of chlorine counterions. For this reason, chlorine counterions were kept in all our calculations with gold clusters.

Since the change in charge is clearly reflected in the distance between the bpy head and thiol tail group, we anchored the $bpy^{2+/\bullet+}$ with two counterions on the three charge states of the Au_{55} cluster. These complexes have two local redox active subunits, the Au_{55} core and the bpy head. Four redox couples are therefore possible as shown in Scheme 1. Three complexes, that differ by the overall charge state $[Au_{55}-S\text{-}link\text{-}bpy\cdot 2Cl]^0$, $[Au_{55}-S\text{-}link\text{-}bpy\cdot 2Cl]^-$, and $[Au_{55}-S\text{-}link\text{-}bpy\cdot 2Cl]^+$ have been investigated. All the structures were relaxed initially in the plane wave approach and the relaxed geometries used as an initial guess for atomic center basis set approach.

In both computational approaches, the presence of one redox active ligand on the bare Au_{55} cluster highly distorts the outer layer of gold atoms and leads to the formation of a cavity for all charged states, as shown in Figure 6a below for the neutral

SCHEME 1: Possible Redox Couples of the Au_{55}^z-S-link-$bpy^{2+/\bullet+}\cdot 2Cl$ Complexes, Where *link* = $(CH_2)_2CO_2(CH_2)_{10}$ and $z = +1$, 0, and -1[a]

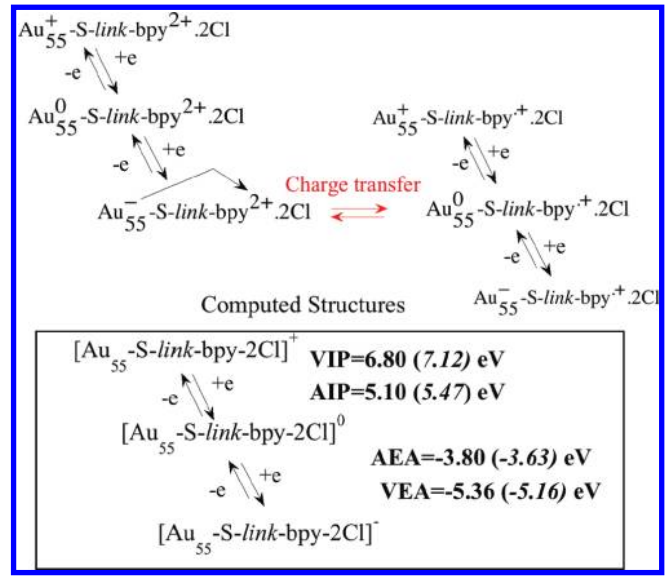

[a] The computed structures are shown in the box. The adiabatic ionization potential (AIP), adiabatic electron affinity (AEA), and vertical electron affinity (VEA) and ionization potential (VIP) are indicated. The values computed in the plane waves approach are reported in italic type.

complex. In order to assess the properties and the reactivity of the cavity, the redox active molecule was partially solvated by one layer of 21 water molecules (Figure 6b). Though the cavity is still present at the outer layer of Au_{55}, the solvent molecules did not enter into the gold cluster. This indicates that this cavity formation could be a structural artifact due to the lack of a densely packed protecting layer around the cluster, which is always present in the experiments and not in this computation. We therefore investigated the structure of the $Au_{55}(SCH_3)_{41}$-$(S(CH_2)_2CO_2(CH_2)_{10}bpy)\cdot 2Cl\cdot 21H_2O$ cluster, for which the cavity formation is completely prevented as shown in the Figure 6c.

In the case of the anchoring of a single redox active ligand on Au_{55}, the Au−S bond distance increases to 2.47 Å compared to Au−S 2.40 Å in the $Au_{55}(SCH_3)_{42}$ cluster because of the electron withdrawing groups. The redox active Au−S bond further increases by 0.02 Å in the thiolated $Au_{55}(SCH_3)_{41}(S(CH_2)_2$-$CO_2(CH_2)_{10}bpy)\cdot 2Cl\cdot 21H_2O$ cluster. As observed for the other complexes, the geometry of the negatively charged $[Au_{55}-S\text{-}link\text{-}bpy\cdot 2Cl]^-$ cluster is less distorted than that of the neutral and positively charged ones. The change in the overall charge of the complex is reflected in the distance between the Au_{55} outer layer gold atoms and the bpy redox active subunit, in both atomic center basis functions/plane wave approaches: $[Au_{55}-S\text{-}link\text{-}bpy\cdot 2Cl]^+$, 5.45/5.43 Å; $[Au_{55}-S\text{-}link\text{-}bpy\cdot 2Cl]^0$, 5.21/5.19 Å; $[Au_{55}-S\text{-}link\text{-}bpy\cdot 2Cl]^-$, 5.01/4.99 Å; see Figure 7. The bond length values in both methods are following the same trend, and the values are comparable. The small difference might be attributed to the absence of exchange term and to the looser convergence criterion used in the plane waves approach. The bond length change upon changing the overall charge of the complex reflects the change in electrostatic repulsion between the Au_{55} cluster and bpy ligand, due to local charge variation on both units. When compared with the single ligand computation, the anchoring of the redox active ligand on the thiolated gold cluster slightly increases the change in distance between

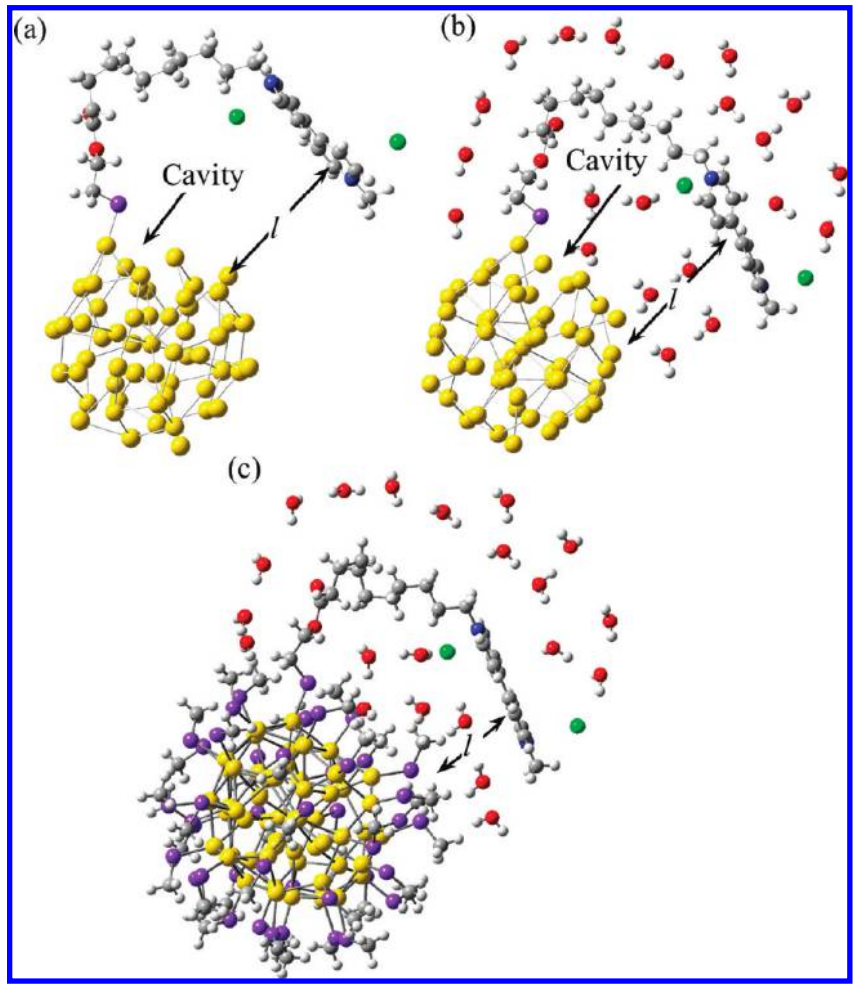

Figure 6. The structure of Au_{55}−S-link-bpy·2Cl (a) and Au_{55}−S-link-bpy·2Cl·0.21H_2O (b), and $Au_{55}(SCH_3)_{41}(S(CH_2)_2CO_2(CH_2)_{10}bpy)$·2Cl·21$H_2O$ (c) complexes, where *link* = $(CH_2)_2CO_2(CH_2)_{10}$. The complex orientation is chosen to show the cavity induced by the ligation of a single redox active ligand. "*l*" represents the distance between the Au_{55} cluster and bpy redox active ligand.

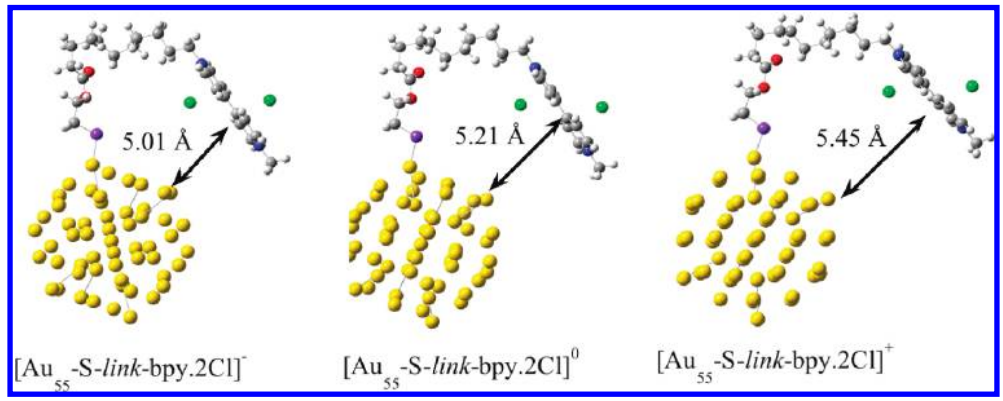

Figure 7. The arm-like motion of the Au_{55} cluster and bpy unit for the three charge states of the $Au_{55}(S(CH_2)_2CO_2(CH_2)_{10}bpy)$·2Cl·21$H_2O$ cluster.

the bpy head unit and the outer layer gold atoms, due to the charge transfer between gold cluster and thiol ligands.

The change in charge is further analyzed by plotting the electron density differences between the neutral $[Au_{55}$−S-*link*-bpy·2Cl$]^0$ and the negatively $[Au_{55}$−S-*link*-bpy·2Cl$]^-$ and positively $[Au_{55}$−S-*link*-bpy·2Cl$]^+$ charged clusters. The removal of one electron leads to a significant hole localization at the Au_{55} unit in the relaxed geometry (Figure 8a) while the addition of an electron localizes the excess negative charge, at both the Au_{55} and bpy unit (Figure 8c). In addition, the charge difference between the $[Au_{55}$−S-*link*-bpy·2Cl$]^0$ and the vertical, diabatic $[Au_{55}$−S-*link*-bpy·2Cl$]^-$ states plotted in Figure 8b shows that in the unrelaxed charged state, the extra electron is localized at the Au_{55} local unit. This clearly indicates the charge transfer from Au_{55} to bpy unit takes place upon geometry relaxation as is observed during the cyclic voltammetric experiment.[13] The same trends are observed in the presence of solvent and of a densely packed $Au_{55}(SCH_3)_{41}(S(CH_2)_2CO_2$-$(CH_2)_{10}bpy)$·2Cl·21$H_2O$ thiol layer. More detailed studies are needed for elucidating the mechanism for charge transfer. The observed 5.0−5.45 Å change in distance between Au_{55} and bpy ligand in three charge states (see Figure 7) for Au_{55}−(S-*link*-

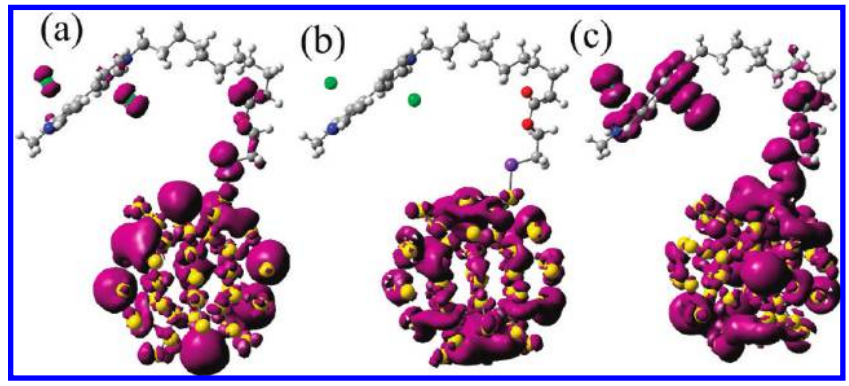

Figure 8. The electron density difference plots. (a) $[Au_{55}-S\text{-}link\text{-}bpy\cdot 2Cl]^0-[Au_{55}-S\text{-}link\text{-}bpy\cdot 2Cl]^+$; (b) vertical $[Au_{55}-S\text{-}link\text{-}bpy\cdot 2Cl]^--[Au_{55}-S\text{-}link\text{-}bpy\cdot 2Cl]^0$; and (c) $[Au_{55}-S\text{-}link\text{-}bpy\cdot 2Cl]^--[Au_{55}-S\text{-}link\text{-}bpy\cdot 2Cl]^0$, where $link = (CH_2)_2CO_2(CH_2)_{10}$.

bpy)·2Cl suggests that it is likely to occur through space rather than through the longer (10−12 Å) linker. In the thiol-passivated complexes $Au_{55}(SCH_3)_{41}(S(CH_2)_2CO_2(CH_2)_{10}bpy)\cdot 2Cl\cdot 21H_2O$, these distances increase from 5.23 Å for negatively charged to 5.39 Å for neutral and 5.57 Å for positively charged clusters, respectively.

IV. Charge Analysis and Electronic Properties

Structural analyses of all the investigated thiol passivated and solvated Au_{55} cluster models show that the outer layer structure of Au_{55} cluster is considerably distorted by the interaction with the thiol ligands and to a lesser extent by the water shell. However, as discussed above, unlike for other sizes of core where RS−Au−SR bridges can form,[12,20−31] the integrity of the outer shell of the Au_{55} metallic cluster is preserved by the dense packing of the thiols.

As was already noted,[12,28,38−40,49] the structural changes are accompanied by a significant charge transfer from the Au_{55} core to the ligand shell.

We report in this section on the charge analysis of all the clusters both in the atomic center basis set method and plane waves approach. Both methods lead to the same results. In the bare Au_{55} cluster, the addition and removal of an electron is affecting the outer layer of gold atoms rather than the inner shell as shown at the bottom part of Figure 9. Both methods predict four types of gold atoms in the bare icosahedral cluster: 1 center, 12 inner shell, 12 outer shell face edge atoms, and 30 outer shell face-centered atoms, which is in agreement with the Mössbauer prediction of the four types of gold atoms.[61] The water solvation of the bare cluster preserves the charge in the center and inner shell of the gold atoms; however a small amount of charge transfer (0.02 e) occurs from the outer layer to the water layer (see top part of Figure 9).

The comparison of the bare and $Au_{55}(SCH_3)_{42}$ ligated cluster Mulliken charges shows that upon passivation a larger charge transfer from the outer shell of gold atoms to the thiol ligand shell (0.2 e) takes place (see Figure 9). The water solvation on the $Au_{55}(SCH_3)_{42}$ cluster reduces the amount of charge transfer to the thiol layer. The reason is that the formation of H-bonds between the thiol groups and water molecules reduces the electron density on the sulfur atoms. Similarly to the bare Au_{55} cluster, the positively charged solvated and ligated clusters have a larger dipole moment (7.4 D) than the neutral (4.3 D) and negatively charged (2.6 D) ones which reflects the amount of distortion of the icosahedral structure.

In addition the negatively charged cluster is always chemically more stable than the neutral and positively charged cluster, which is reflected in the energy differences between the frontier

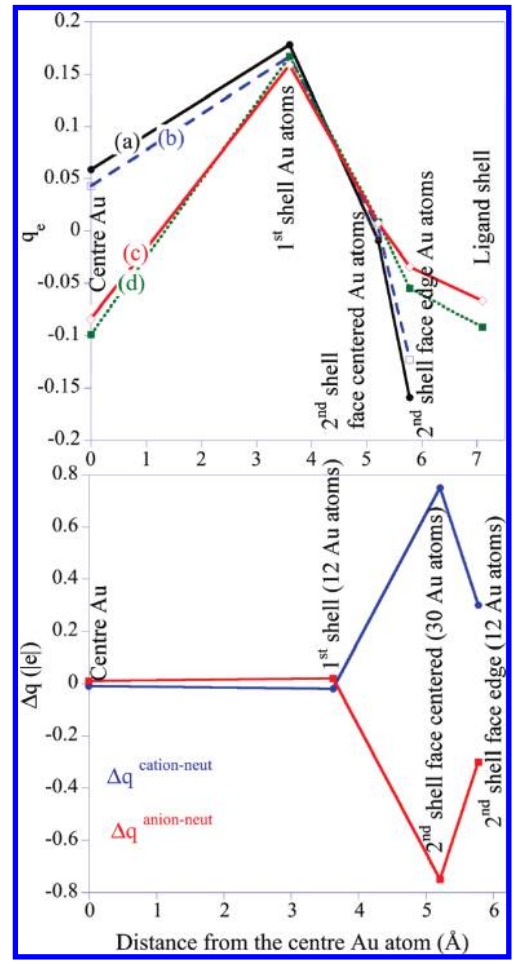

Figure 9. (Top) Comparison of the averaged charge on the different kinds of Au atoms and ligand shell for Au_{55} (a), $Au_{55}\cdot 54H_2O$ (b), $Au_{55}(SCH_3)_{42}$ (c), and $Au_{55}(SCH_3)_{42}\cdot 54H_2O$ (d). (Bottom) Difference between the cumulative charge carried by the four types of atoms for the cation and the neutral (filled circles) and the anion and the neutral (filled squares) in bare cluster.

orbitals, $\Delta = E_{LUMO} - E_{HOMO}$ (see Table 1). The Δ values are tabulated together with the atomic orbital contributions to the frontier molecular orbitals. The Δ values are indicative of the chemical reactivity of the clusters and the atomic orbital contributions of the outer layer of gold atoms reflect the strength of ligand effects.

For the neutral bare and all investigated redox inactive ligated $Au_{55}(SCH_3)_{42}$ clusters, the value of Δ for the α MO's (Δ = 1.3 eV) of the neutral is about equal to the value of Δ for the anion (1.4 eV) and that of the β MO (0.98 eV) to that of the cation

TABLE 1: The Diameter and the Atomic Orbital Contributions to the HOMO of the Bare and $Au_{55}(SCH_3)_{42}$, $Au_{55}(SCH_3)_{42}\cdot 54H_2O$ (see Figures 1 and 2) Computed in the Atomic Center Basis Set Computation and Atomic Orbital Contribution of [Au_{55}−S-*link*-bpy] and [Au_{55}−S-*link*-bpy·2Cl·$21H_2O$] Computed in the Plane Waves Approach, where link = $(CH_2)_2CO_2(CH_2)_{10}$

clusters	diameter of the Au_{55} core (nm)	atomic orbital contribution to the HOMO: face edge Au 6s (%)	face edge Au 5d (%)	face center Au 6s (%)	face center Au 5d (%)	Δ (eV)
Au_{55}^+	1.14	21	24	4	41	0.98
Au_{55}^0	1.15	33	7	3	50	(α) 1.30 and (β) 0.98
Au_{55}^-	1.15	53	6	5	29	1.40
$[Au_{55}\cdot 54H_2O]^+$	1.21	19	18	4	35	0.86
$[Au_{55}\cdot 54H_2O]^0$	1.19	28	2	3	44	(α) 1.28 and (β) 0.90
$[Au_{55}\cdot 54H_2O]^-$	1.20	41	5	2	12	1.32
$[Au_{55}(SCH_3)_{42}]^+$	1.26	5	21	3	19	0.27
$[Au_{55}(SCH_3)_{42}]^0$	1.25	10	11	4	16	(α) 0.89 and (β) 0.33
$[Au_{55}(SCH_3)_{42}]^-$	1.23	18	6	6	12	0.96
$[Au_{55}(SCH_3)_{42}\cdot 54H_2O]^+$	1.28	3	29	2	16	0.40
$[Au_{55}(SCH_3)_{42}\cdot 54H_2O]^0$	1.26	6	9	1	19	(α) 0.91 and (β) 0.42
$[Au_{55}(SCH_3)_{33}\cdot 54H_2O]^-$	1.25	15	5	4	9	1.01
[Au_{55}−S-*link*-bpy.2Cl]$^+$	1.34	10	16	10	15	(α) 0.366 and (β) 0.107
[Au_{55}−S-*link*-bpy·2Cl]^0	1.33	6	2	5	9	0.134
[Au_{55}−S-*link*-bpy·2Cl]$^-$	1.31	3	2	7	2	(α) 0.396 and (β) 0.157
[Au_{55}−S-*link*-bpy·2Cl·$21H_2O$]$^+$	1.37	9	13	5	121	(α) 0.249 and (β) 0.251
[Au_{55}−S-*link*-bpy·2Cl·$21H_2O$]^0	1.35	7	12	5	1.5	0.496
[Au_{55}−S-*link*-bpy·2Cl·$21H_2O$]$^-$	1.33	6	9	2		(α) 0.776 and (β) 0.554

(0.98 eV). This shows that there is no extensive electronic relaxation upon adding or removing an electron to the neutral Au_{55}. However, the negatively charged nanoclusters, bare and ligated, are more stable than the other charged forms as indicated by their higher Δ values.

In $Au_{55}(SCH_3)_{42}$, the addition of the ligand shell decreases the HOMO−LUMO gap by 0.5 eV. In the frontier orbitals (Figure 10), we note a significant contribution (37%) of the 3p S orbitals indicating that the S atoms strongly interact with the Au_{55} core. The antibonding nature of the Au−S bonds in the HOMO and LUMO clearly reflects the 5d−3p back bonding effect. The bonding to the SCH_3 ligands is accompanied by a significant charge transfer, as reflected by the computed Mulliken charges, which are slightly positive on the Au atoms and slightly negative on the SCH_3 groups. Note that the ligation of each gold atom in the outer layer is uniform, and therefore the four types of gold atoms that we characterized in the bare Au_{55} (see Figure 2) are preserved in the ligated and solvated clusters: (i) 1 center, (ii) 12 first shell, (iii) 12 face center, and 20 face edge outer layer gold atoms.

We now turn to the analysis of the charge reorganization in the case of the complexes with the bpy redox active ligand. The addition of an electron to the Au_{55}−S-*link*-bpy cluster is accompanied by a significant amount of charge transfer to the bpy ligand. Figure 8 above shows the computed total electron density difference between the neutral [Au_{55}−S-*link*-bpy·2Cl]^0 and the corresponding positively and negatively charged clusters. The addition of an electron without geometry relaxation (vertical attachment) to form the [Au_{55}−S-*link*-bpy·2Cl]$^-$ cluster leads to the formation of a species where the maximum excess negative charge is localized at the Au_{55} subunit (Figure 8b).

V. Electrical Properties Analysis

The difference in hybridization of the frontier orbitals for the different charge states explains the large computed value of the ionization energies (IP = $E(N-1) - E(N)$) (4−7 eV) and the low value of the electron affinity (EA = $E(N+1) - E(N)$) (−4 to −11 eV) of the bare and ligated clusters. On the other hand, the charging energy (CE) values, obtained as IP + EA, govern the conducting and insulator nature of the clusters (see Table 2). The computed value for the charging energy of the bare cluster is $CE_{bare} = 2.02$ eV. The presence of a solvation shell decreases this value by 0.75 eV, $CE_{Au_{55}\cdot 54H_2O} = 1.27$ eV.

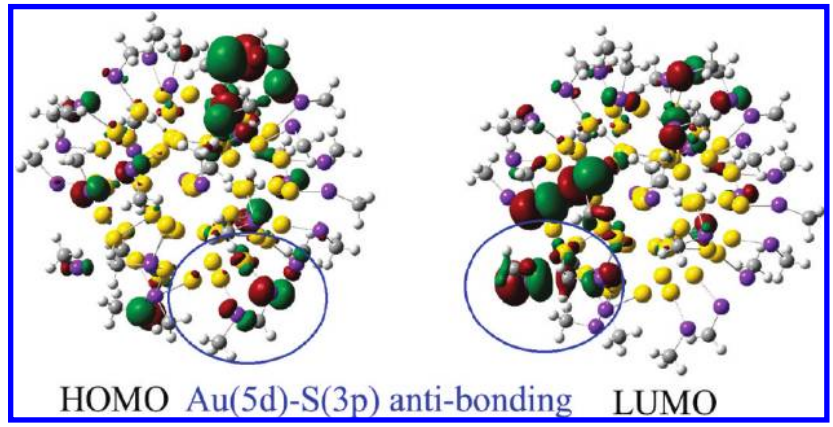

Figure 10. Frontier molecular orbitals (HOMO and LUMO) of neutral $Au_{55}(SCH_3)_{42}$ cluster computed at the atomic center basis functions. For clarity a Au−S bond is marked by the circle.

TABLE 2: Calculated Electronic Properties (eV) for Bare and Various Ligated Model Clusters[a]

	IP	EA	U_c
Au_{55}	6.36	–4.34	2.02
$Au_{55}\cdot 54H_2O$	6.09	–4.82	1.27
$Au_{55}(SCH_3)_{42}$	7.08	–3.84	3.24
$Au_{55}(SCH_3)_{42}\cdot 54H_2O$	4.03	–2.85	1.18
[Au_{55}–S-*link*-bpy·2Cl]	5.10	–3.80	
[Au_{55}-$(SCH_3)_{41}$(S-*link*-bpy)·2Cl·21H_2O]	4.23	–3.42	

[a] The adiabatic IP is computed as $E(N-1)-E(N)$, the adiabatic EA as $E(N+1)-E(N)$ and the charging energy U_c as EA + IP = $E(N+1)-2E(N)+E(N-1)$. The values are reported in eV.

Due to the strong covalent bonds between the gold cluster and the thiol ligands, the charging energy increases for the thiol passivated $Au_{55}(SCH_3)_{42}$, $CE_{Au_{55}(SCH_3)_{42}} = 3.24$ eV. This value, computed for a gas phase complex, indicates an insulating behavior with a large conduction gap. In order to be able to compare with the experimental value of 0.3−0.5 eV, one has to take the solvent effect into account. The charging energy decreases to CE = 1.18 eV for $Au_{55}(SCH_3)_{42}\cdot 54\ H_2O$, which is in good agreement with the experimental range of values. Note that as discussed in detail above, the addition of a water layer does not effect the structure of the clusters much so that the spherical model estimation of the capacitance, $CE = 4\pi\varepsilon\varepsilon_0(r/d)(r+d)$,[4] where $r = 0.63$ nm; $d = 0.24$ nm and dielectric constant of the water solvated thiol layer ($\varepsilon = 3.0$) results in a value of 0.914 eV that is in good agreement with the computed one.

The computed adiabatic ionization potential (7.08 eV) and electron affinity (−3.84 eV) values for $Au_{55}(SCH_3)_{42}$ are comparable with the values reported values for $Au_{38}(SCH_3)_{24}$ (IP: 5.31 eV and EA:−3.41 eV).[28] The larger ionization potential value is due to the high distortion of the outer layer that we observe for the positively charged cluster.

We have also computed the redox potential values for the Au_{55} cluster with a anchored redox active ligand. The values of the redox couple for [Au_{55}−S-*link*-bpy·2Cl]$^+$/[Au_{55}−S-*link*-bpy·2Cl]^0 and [Au_{55}−S-*link*-bpy·2Cl]^0/[Au_{55}−S-*link*-bpy·2Cl]$^-$ are 5.10 and 3.80 eV, respectively, which leads to a difference of 1.3 eV. When computed in the presence of dense thiol layer and 21 water molecules around the bpy and Au_{55} subunits, the redox potential difference becomes 0.81 eV, in good agreement with the reported experimental value of 1 eV.[13] The difference between computed and experimental values could be due to the absence of a complete water layer.

Further the electron transfer from Au_{55} to bpy unit is also in agreement with the values of the local redox potentials of the functional units in the [Au_{55}−S-*link*-bpy·2Cl] cluster since both Au_{55} and bpy units are separated by a long linker. The computed adiabatic redox potential for the isolated $bpy^{2+}/bpy^{\bullet+}$ couple discussed above is 3.94 eV, and it is 4.82 eV for the Au_{55}^0/Au_{55}^- couple. This leads a negative ΔE of 1 eV, which shows that the process is thermodynamically allowed. On the other hand, no charge transfer can take place for the positively charged [Au_{55}−S-*link*-bpy·2Cl]$^+$ cluster due to wrong ordering of the ionization potential compared with that of the bpy unit.

Computational aspects that are expected to further decrease the value of the charging energy are the use of a basis set larger than the 6-31+G(d) basis used here in order to better describe the H-bonding and the addition of a second shell of water molecules. Both improvements lead to serious convergence problems for the geometry relaxation and are computationally prohibitive at this stage. In addition, the value of the charging energy will be further decreased by the interaction with neighboring clusters.

Conclusions

Our computational study shows that the more stable icosahedral geometry of Au_{55} in the bare form is preserved upon ligation and solvation in the neutral, negative, and positive charge states, leading to the presence of four different types of gold atoms as reported by Mössbauer studies.[61] Upon ligation by thiol ligand, a significant charge transfer occurs from the outer shell of the Au_{55} to the ligand shell, which leads to a more insulating behavior of the passivated unsolvated cluster and a larger value of the charging energy (3.24 eV for $Au_{55}(SCH_3)_{42}$ compared to 2.02 eV for Au_{55}). A more metallic character and charging energy values comparable to experimental ones (≈1.2 eV compared to the experimental 0.3−0.5 eV reported values) are recovered when explicit solvation effects are included. The anchoring of a bpy redox active ligand on the thiolated $Au_{55}(SCH_3)_{42}$ cluster leads to a redox process for the negatively charged [Au_{55}-$(SCH_3)_{41}$(S-*link*-bpy)·2Cl·21H_2O]$^-$. The geometry relaxation upon localizing a negative charge on the Au_{55} core is accompanied by a charge transfer from the Au_{55}^- unit to the bpy^{2+} one. The computed redox potential as well as the decrease of the distance between the Au_{55} core and the bpy^{2+} unit upon changing the overall charge from positive to neutral to negative are in agreement with experimental results.

Acknowledgment. This work is supported by the EC FP7MOLOC project and the FRFC 2.4506 project. The work of GP and ED is supported by an Inter University Attraction Pole (IAP) project "Cluster and Nanowires" of the Belgian federal government. FR and JYR also belong to FNRS, Belgium. We thank R. D. Levine (HUJI, Israel), I. Willner (HUJI, Israel) and E. S. Kryachko (ULg, Belgium and Bogolyubov Institute for Theoretical Physics, Kiev) for several insightful discussions.

Supporting Information Available: Additional figures and a table comparing computed values for the plane wave and atomic center basis set approach. This information is available free of charge via the Internet at http://pubs.acs.org.

References and Notes

(1) Simon, U.; Schon, G.; Schmid, G. *Angew. Chem., Int. Ed.* **1993**, *32* (2), 250–254.
(2) Schmid, G. *Chem. Soc. Rev.* **2008**, *37* (9), 1909–1930.
(3) Yam, V. W. W.; Cheng, E. C. C. *Chem. Soc. Rev.* **2008**, *37* (9), 1806–1813.
(4) Murray, R. W. *Chem. Rev.* **2008**, *108* (7), 2688–2720.
(5) Jin, R. *Nanoscale* **2010**, published on line, DOI: 10.1039/b9nr00160c.
(6) Schmid, G.; Klein, N.; Korste, L.; Kreibig, U.; Schonauer, D. *Polyhedron* **1988**, *7* (8), 605–608.
(7) Schmid, G.; Pugin, R.; Meyer-Zaika, W.; Simon, U. *Eur. J. Inorg. Chem.* **1999**, (11), 2051–2055.
(8) Tsunoyama, H.; Negishi, Y.; Tsukuda, T. *J. Am. Chem. Soc.* **2006**, *128* (18), 6036–6037.
(9) Hanaoka, T.; Kormann, H. P.; Kroll, M.; Sawitowski, T.; Schmid, G. *Eur. J. Inorg. Chem.* **1998**, (6), 807–812.
(10) Crookes-Goodson, W. J.; Slocik, J. M.; Naik, R. R. *Chem. Soc. Rev.* **2008**, *37* (11), 2403–2412.
(11) Grzelczak, M.; Perez-Juste, J.; Mulvaney, P.; Liz-Marzan, L. M. *Chem. Soc. Rev.* **2008**, *37* (9), 1783–1791.
(12) Jiang, D. E.; Nobusada, K.; Luo, W. D.; Whetten, R. L. *ACS Nano* **2009**, *3* (8), 2351–2357.
(13) Wang, X. M.; Kharitonov, A. B.; Katz, E.; Willner, I. *Chem. Commun.* **2003**, (13), 1542–1543.
(14) Baron, R.; Onopriyenko, A.; Katz, E.; Lioubashevski, O.; Willner, I.; Sheng, W.; Tian, H. *Chem. Commun.* **2006**, (20), 2147–2149.
(15) Katz, M. J.; Sakai, K.; Leznoff, D. B. *Chem. Soc. Rev.* **2008**, *37* (9), 1884–1895.

(16) Boyen, H. G.; Kastle, G.; Weigl, F.; Ziemann, P.; Schmid, G.; Garnier, M. G.; Oelhafen, P. *Phys. Rev. Lett.* **2001**, *87* (27, pt.1), 276401/1-4.
(17) Boyen, H. G.; Kastle, G.; Weigl, F.; Koslowski, B.; Dietrich, C.; Ziemann, P.; Spatz, J. P.; Riethmuller, S.; Hartmann, C.; Moller, M.; Schmid, G.; Garnier, M. G.; Oelhafen, P. *Science* **2002**, *297* (5586), 1533–1536.
(18) Schmidbaur, H.; Schier, A. *Chem. Soc. Rev.* **2008**, *37* (9), 1931–1951.
(19) Jiang, D. E.; Whetten, R. L.; Luo, W. D.; Dai, S. *J. Phys. Chem. C* **2009**, *113* (40), 17291–17295.
(20) Jadzinsky, P. D.; Calero, G.; Ackerson, C. J.; Bushnell, D. A.; Kornberg, R. D. *Science* **2007**, *318*, 430–433.
(21) Li, Y.; Galli, G.; Gygi, F. *ACS Nano* **2008**, *2* (9), 1896–1902.
(22) Heaven, M. W.; Dass, A.; White, P. S.; Holt, K. M.; Murray, R. W. *J. Am. Chem. Soc.* **2008**, *130* (12), 3754–3755.
(23) Zhu, M.; Aikens, C. M.; Hollander, F. J.; Schatz, G. C.; Jin, R. *J. Am. Chem. Soc.* **2008**, *130* (18), 5883–5885.
(24) Akola, J.; Walter, M.; Whetten, R. L.; Hakkinen, H.; Gronbeck, H. *J. Am. Chem. Soc.* **2008**, *130* (12), 3756–3757.
(25) Wang, W.; Lee, D.; Murray, R. W. *J. Phys. Chem. B* **2006**, *110* (21), 10258–10265.
(26) Qian, H.; Zhu, Y.; Jin, R. *ACS Nano* **2009**, *3* (11), 3795–3803.
(27) Hakkinen, H.; Walter, M.; Gronbeck, H. *J. Phys. Chem. B* **2006**, *110* (20), 9927–9931.
(28) Hakkinen, H.; Barnett, R. N.; Landman, U. *Phys. Rev. Lett.* **1999**, *82* (16), 3264–3267.
(29) Walter, M.; Akola, J.; Lopez-Acevedo, O.; Jadzinsky, P. D.; Calero, G.; Ackerson, C. J.; Whetten, R. L.; Gronbeck, H.; Hakkinen, H. *Proc. Natl. Acad. Sci. U.S.A.* **2008**, *105* (27), 9157–9162.
(30) Qian, H.; Jin, R. *Nano Lett.* **2009**, *9* (12), 4083–4087.
(31) Lopez-Acevedo, O.; Akola, J.; Whetten, R. L.; Gronbeck, H.; Hakkinen, H. *J. Phys. Chem. C* **2009**, *113* (13), 5035–5038.
(32) Pyykko, P. *Angew. Chem., Int. Ed.* **2004**, *43* (34), 4412–4456.
(33) Hakkinen, H.; Yoon, B.; Landman, U.; Li, X.; Zhai, H. J.; Wang, L. S. *J. Phys. Chem. A* **2003**, *107* (32), 6168–6175.
(34) Koskinen, P.; Hakkinen, H.; Seifert, G.; Sanna, S.; Frauenheim, T.; Moseler, M. *New J. Phys.* **2006**, *8* (1), .
(35) Xiao, L.; Tollberg, B.; Hu, X. K.; Wang, L. C. *J. Chem. Phys.* **2006**, 124.
(36) Pauly, F.; Viljas, J. K.; Huniar, U.; Hafner, M.; Wohlthat, S.; Burkle, M.; Cuevas, J. C.; Schon, G. *New J. Phys.* **2008**, 10.
(37) Jensen, L.; Aikens, C. M.; Schatz, G. C. *Chem. Soc. Rev.* **2008**, *37* (5), 1061–1073.
(38) Pérez, L. A.; López-Lozano, X.; Garzón, I. L. *Eur. Phys. J. D* **2009**, *52*, 123–126.
(39) Jiang, D. E.; Whetten, R. L. *Phys. Rev. B* **2009**, *80* (11), 5.
(40) Hakkinen, H. *Chem. Soc. Rev.* **2008**, *37* (9), 1847–1859.
(41) Pyykko, P. *Chem. Soc. Rev.* **2008**, *37* (9), 1967–1997.
(42) Hakkinen, H.; Moseler, M.; Landman, U. *Phys. Rev. Lett.* **2002**, *89* (3), .
(43) Hakkinen, H.; Moseler, M.; Kostko, O.; Morgner, N.; Hoffmann, M. A.; von Issendorff, B. *Phys. Rev. Lett.* **2004**, 93.
(44) Frisch, M. J.; Trucks, G. W.; Schlegel, H. B.; Scuseria, G. E.; Robb, M. A.; Cheeseman, J. R.; J. A. Montgomery, J.; Vreven, T.; Kudin, K. N.; Burant, J. C.; Millam, J. M.; Iyengar, S. S.; Tomasi, J.; Barone, V.; Mennucci, B.; Cossi, M.; Scalmani, G.; Rega, N.; Petersson, G. A.; Nakatsuji, H.; Hada, M.; Ehara, M.; Toyota, K.; Fukuda, R.; Hasegawa, J.; Ishida, M.; Nakajima, T.; Honda, Y.; Kitao, O.; Nakai, H.; Klene, M.; Li, X.; Knox, J. E.; Hratchian, H. P.; Cross, J. B.; Adamo, C.; Jaramillo, J.; Gomperts, R.; Stratmann, R. E.; Yazyev, O.; Austin, A. J.; Cammi, R.; Pomelli, C.; Ochterski, J. W.; Ayala, P. Y.; Morokuma, K.; Voth, G. A.; Salvador, P.; Dannenberg, J. J.; Zakrzewski, V. G.; Dapprich, S.; Daniels, A. D.; Strain, M. C.; Farkas, O.; Malick, D. K.; Rabuck, A. D.; Raghavachari, K.; Foresman, J. B.; Ortiz, J. V.; Cui, Q.; Baboul, A. G.; Clifford, S.; Cioslowski, J.; Stefanov, B. B.; Liu, G.; Liashenko, A.; Piskorz, P.; Komaromi, I.; Martin, R. L.; Fox, D. J.; Keith, T.; Al-Laham, M. A.; Peng, C. Y.; Nanayakkara, A.; Challacombe, M.; Gill, P. M. W.; Johnson, B.; Chen, W.; Wong, M. W.; Gonzalez, C.; Pople, J. A. *Gaussian 03, Revision C.02*; Gaussian, Inc.: Wallingford CT, 2003.
(45) Case, D. A.; Darden, T. A.; T.E. Cheatham, I.; Simmerling, C. L.; Wang, J.; Duke, R. E.; Luo, R.; Crowley, M.; Walker, R. C.; Zhang, W.; Merz, K. M.; Wang, B.; Hayik, S.; Roitberg, A.; Seabra, G.; Kolossváry, I.; Wong, K. F.; Paesani, F.; Vanicek, J.; Wu, X.; Brozell, S. R.; Steinbrecher, T.; Gohlke, H.; Yang, L.; Tan, C.; Mongan, J.; Hornak, V.; Cui, G.; Mathews, D. H.; Seetin, M. G.; Sagui, C.; Babin, V.; Kollman, P. A., *AMBER 10.*: University of California: San Francisco, 2008.
(46) Kresse, G.; Furthmuller, J. *Phys. Rev. B* **1996**, *54*, 11169.
(47) Kresse, G.; Hafner, J. *Phys. Rev. B* **1993**, *47*, 558.
(48) Blöchl, P. E. *Phys. Rev. B* **1994**, *50*, 17953.
(49) Periyasamy, G.; Remacle, F. *Nano Lett.* **2009**, *9* (8), 3007–3011.
(50) Miyauchi, H.; Taketomi, K.; Egami, A.; Hosoi, S.; Fukutani, H. *Jpn. J. Appl. Phys., Part 2* **1994**, *34*, 19–21.
(51) Vanderputten, D.; Zanoni, R. *Phys. Lett. A* **1995**, *208* (4−6), 345–350.
(52) Becker, C.; Fries, T.; Wandelt, K.; Kreibig, U.; Schmid, G. *J. Vac. Sci. Technol., B* **1991**, *9* (2), 810–813.
(53) Houbertz, R.; Feigenspan, T.; Mielke, F.; Memmert, U.; Hartmann, U.; Simon, U.; Schon, G.; Schmid, G. *Europhys. Lett.* **1994**, *28* (9), 641–646.
(54) Vandeleemput, L. E. C.; Gerritsen, J. W.; Rongen, P. H. H.; Smokers, R. T. M.; Wierenga, H. A.; Vankempen, H.; Schmid, G. *J. Vac. Sci. Technol., B* **1991**, *9* (2), 814–819.
(55) Schmid, G.; Simon, U. *Chem. Commun.* **2005**, (6), 697–710.
(56) Vogel, W.; Rosner, B.; Tesche, B. *J. Phys. Chem.* **1993**, *97* (45), 11611–11616.
(57) Benfield, R. E.; Filipponi, A.; Bowron, D. T.; Newport, R. J.; Gurman, S. J. *J. Phys.: Condens. Matter* **1994**, *6* (41), 8429–8448.
(58) Fairbanks, M. C.; Benfield, R. E.; Newport, R. J.; Schmid, G. *Solid State Commun.* **1990**, *73* (6), 431–436.
(59) Brom, H. B.; Baak, J.; Dejongh, I. J.; Mulder, F. M.; Thiel, R. C.; Schmid, G. *Z. Phys. D: At., Mol Clusters* **1993**, *26*, S27–S29.
(60) Zhang, H.; Mautes, D.; Hartmann, U. *New J. Phys.* **2003**, 5.
(61) Sawada, S.; Sugano, S. *Z. Phys. D: At., Mol Clusters* **1992**, *24* (4), 377–384.
(62) Hakkinen, H.; Moseler, M. *Comput. Mater. Sci.* **2006**, *35* (3), 332–336.
(63) Cramer, J. C., *Theories and Models.*, 2nd ed.; John Wiley & sons Ltd.: Chichester, England: p 205.
(64) Kryachko, E. S.; Remacle, F. *Chem. Phys. Lett.* **2005**, *404* (1−3), 142–149.
(65) Kryachko, E. S.; Remacle, F. *Nano Lett.* **2005**, *5* (4), 735–739.
(66) Kryachko, E. S.; Remacle, F. *J. Chem. Phys.* **2007**, 127.
(67) Abe, M.; Kondo, T.; Uosaki, K.; Sasaki, Y. *J. Electroanal. Chem.* **1999**, *473* (1−2), 93–98.
(68) Zhang, J. D.; Chi, Q. J.; Nielsen, J. U.; Friis, E. P.; Andersen, J. E. T.; Ulstrup, J. *Langmuir* **2000**, *16* (18), 7229–7237.
(69) Gittins, D. I.; Bethell, D.; Nichols, R. J.; Schiffrin, D. J. *J. Mater. Chem.* **2000**, *10* (1), 79–83.
(70) Horswell, S. L.; O'Neil, I. A.; Schiffrin, D. J. *J. Phys. Chem. B* **2003**, *107* (20), 4844–4854.
(71) Chen, S.; Deng, F. J. *Langmuir* **2002**, *18* (23), 8942–8948.
(72) Michi, T.; Abe, M.; Matsuno, J.; Uosaki, K.; Sasaki, Y. *Bull. Chem. Soc. Jpn.* **2007**, *80*, 1368–1376.
(73) Sasaki, Y.; Abe, M. *Chem. Rec.* **2004**, *4* (5), 279–290.
(74) Tomiyasu, Y.; Abe, M.; Morihara, Y.; Ohgi, H.; Otake, T.; Hisaeda, Y. *Chem. Lett.* **2009**, *38* (5), 492–493.
(75) Albrecht, T.; Mertens, S. F. L.; Ulstrup, J. *J. Am. Chem. Soc.* **2007**, *129* (29), 9162–9167.
(76) Zhang, J. D.; Kuznetsov, A. M.; Medvedev, I. G.; Chi, Q. J.; Albrecht, T.; Jensen, P. S.; Ulstrup, J. *Chem. Rev.* **2008**, *108* (7), 2737–2791.

JP9119827